Journal of Materials Research and Technology 33 (2024) 9802–9810

Contents lists available at ScienceDirect

Journal of Materials Research and Technology

journal homepage: www.elsevier.com/locate/jmrt

Effect of building direction and heat treatment on the wear behavior of H13 tool steel processed by laser powder bed fusion

Adriel P. Oliveira [a,*], Tales Ferreira [a], Reginaldo T. Coelho [b], Claudemiro Bolfarini [a,c], Piter Gargarella [a,c,d]

[a] Federal University of São Carlos, Graduate Program in Materials Science and Engineering, Rod. Washington Luiz, Km 235 SP-310, 13565-905, São Carlos, SP, Brazil
[b] Department of Production Engineering, São Carlos Engineering School, University of São Paulo, Av. Trabalhador São-Carlense, 400, 13566-590, São Carlos, SP, Brazil
[c] Federal University of São Carlos, Department of Materials Engineering, Rod. Washington Luiz, Km 235 SP-310, 13565-905, São Carlos, SP, Brazil
[d] Center of Characterization and Development of Materials, Federal University of São Carlos, Rod. Washington Luiz, km 235 SP-310, 13565-905, São Carlos, SP, Brazil

ARTICLE INFO

Keywords:
Hot work tool steel
Laser powder bed fusion
Wear resistance

ABSTRACT

Components such as molds and dies face the challenge of costly preparation due to their complex geometry. However, Additive Manufacturing offers unprecedented design freedom for these tools. In this study, AISI H13 hot work tool steel was processed by laser powder bed fusion (L-PBF) and subjected to reciprocal wear tests against Al2O3 pin in a sphere-on-plate configuration to evaluate its wear behavior. Comparative analyses were conducted with the same material processed by arc melting (560HV). The microstructure of the printed H13 revealed a cellular morphology, characterized by martensite cells enveloped in retained austenite (556HV). This microstructure was transformed into tempered martensite after heat treatment, maintaining the hardness in the same range (547HV). As-printed samples exhibited a Coefficient of Friction (COF) between 0.72 and 0.85, while heat-treated samples showed a reduced range of 0.72 < COF <0.76. The specific wear rate showed a slight variation between different building directions in the as-printed conditions, with values of 1.7×10^{-4} and 1.2×10^{-4} mm³/N·m for perpendicular and parallel directions to the building direction, respectively. These wear rates were marginally inferior to conventionally processed material (2.2×10^{-4} mm³/N·m). Notably, the printed sample with post-hardening heat treatment exhibited the highest wear rate (3.0×10^{-4} mm³/N·m) compared to as-printed and arc-melted counterparts. Across all conditions, abrasion, adhesion, and delamination were identified as the prevalent wear mechanisms. The findings emphasize the feasibility of manufacturing H13 parts with complex geometries while preserving excellent wear properties, even prior to thermal treatment.

1. Introduction

Hot work tool steels represent a crucial class of materials employed in various material processing applications. These steels must possess robust mechanical strength and toughness to endure cyclic and thermal stresses during operation. Furthermore, their wear resistance is paramount for prolonging their operational lifespan and mitigating costs associated with tool maintenance [1,2].

In recent years, the advancement of additive manufacturing (AM) technologies has garnered special attention for the production of tool steels [3,4]. Traditional manufacturing processes for certain tools involve multiple steps and often restrict the fabrication of parts with intricate geometries. Moreover, in some cases, over 50% of the initial tool material can be lost in machining processes [1]. AM, by enabling the production of parts with complex geometries and internal coolant channels, has the potential to reduce tool industry costs and enhance tool performance by minimizing lead times and delivery times [5,6]. Among the materials utilized in tool production, AISI H13 tool steel has attracted significant research attention due to its versatility in manufacturing dies for diverse processes, including die casting, forging, extrusion, and cutting tools, among others.

Laser powder bed fusion (L-PBF) is a prominent AM technique extensively studied for H13 steel. Numerous correlations between process parameters, microstructure, and mechanical properties such as hardness, tensile strength, impact strength, and bending have been explored in this context [7–13]. However, literature addressing the wear

* Corresponding author. Departamento de Engenharia de Materiais, Universidade Federal de São Carlos, São Carlos, Rod. Washington Luiz, km 235, São Carlos, SP, 13565-905, Brazil.
E-mail address: adrielpugliesi@ppgcem.ufscar.br (A.P. Oliveira).

https://doi.org/10.1016/j.jmrt.2024.12.012
Received 11 September 2024; Received in revised form 8 November 2024; Accepted 1 December 2024
Available online 3 December 2024

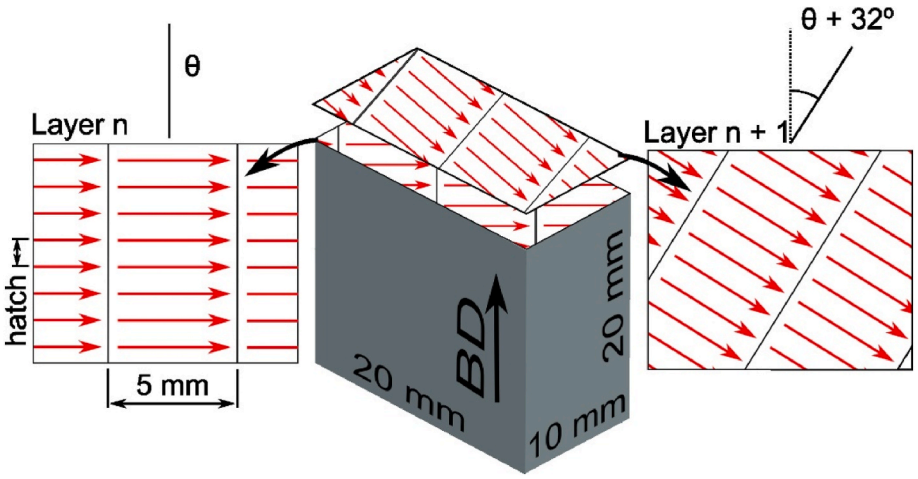

Fig. 1. The scanning strategy employed in this study comprises 5 mm-wide strips with a unidirectional laser movement. The layer thickness was set at 30 μm, and for each subsequent layer, the pattern rotates 32° to the right. BD = building direction.

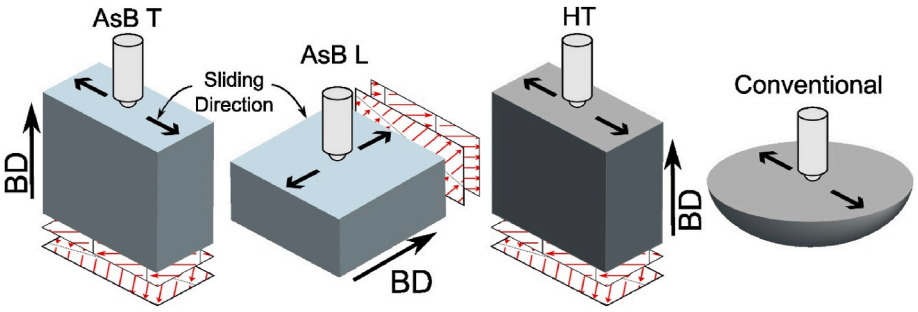

Fig. 2. Scheme showing the sliding direction of wear tests in relation to the 3D printing strategy. BD = building direction.

Table 1
Operating conditions adopted for carrying out the wear tests (Procedure A prescribed by ASTM G133-05 standard).

Sliding conditions	Standard	Applied
Pin tip radius	4.76 mm	5.2 mm
Load	25 N	25 N
Stroke length	10 mm	10 mm
Frequency	5 Hz	5 Hz
Distance	100 m	100 m
Duration	16.7 min	16.7 min
Average sliding speed	0.1 ms^{-1}	0.1 ms^{-1}
Relative humidity	50 ± 10%	51 ± 8%
Temperature	22 ± 3 °C	21 ± 2 °C
Lubrication	None applied	None applied

resistance properties of H13 steel processed by L-PBF remains limited.

In the realm of conventional production processes, the wear properties of H13 steel have been investigated by various researchers. Bahrami et al. [14] conducted a study to examine the impact of heat treatment on the wear resistance of H13 steel, using a pin-on-disk configuration with a roll-bearing steel pin (65 HRC). Their findings revealed that for loads of 29 N, after 1000 m of sliding distance, the quenched H13 steel loses less weight due to wear (around 0.03 g) compared to the tempered H13 steel (0.04 g). However, for a load of 98 N after 1000 m, the tempered condition experienced less weight loss (0.05 g) compared to the quenched condition (0.07 g). Wei et al. [15] studied the combined influence of different tempering temperatures and different test temperatures in wear tests using an H13 pin on a D2 steel disk with a sliding distance of 1200 m. They showed that at room temperatures, the wear mechanism is predominantly adhesive, while at temperatures of 200 °C–400 °C, it becomes oxidative. Wei et al. also demonstrated that the wear rate for the tests at room temperature varied significantly according to the tempering temperature of the piece, being maximum (10×10^{-5} mg/mm) for tempering at 500 °C and minimum (3.5×10^{-5} mg/mm) for tempering at 600 °C [15].

Chen et al. [16] used carborundum sandpapers to wear down H13 pins in a pin-on-disk configuration. The authors demonstrated that modifications made by laser processing on the surface of H13 steel can reduce weight loss by around 57%, depending on the surface condition, through increased surface hardness. Telasang et al. [17] studied the wear resistance of different laser-hardened or remelted H13 surfaces against an alumina ball. They observed that the processing reduced the specific wear rate from $22.5 \times 10^{\wedge -5}$ mm^3/N.m to approximately $1 \times 10^{\wedge -5}$ mm^3/N.m after 150 m of sliding distance, considering a rotating ball-on-disk test under a load of 20 N. The friction coefficient was also reduced from values between 0.75 and 0.9 to values between 0.5 and 0.6. Karmakar et al. [18] conducted different tempering heat treatments on laser-melted H13 surfaces and evaluated their properties through ball-on-disk wear tests using a WC ball. They noticed that laser remelting enhances both surface hardness and wear resistance, following a similar pattern as the hardness observed under different tempering conditions, where increased surface hardness correlates with greater wear resistance. Guenther et al. [19] conducted pin-on-disk wear tests on H13 parts produced by additive manufacturing, using mineral base oil lubrication, and varying surface finishes and laser surface texturing. The counterbody was a disk of AISI 5210 bearing steel. The friction coefficient values exhibited a range of results, starting at 0.14 for the textured samples, decreasing to 0.11 for the as-printed samples, and eventually reaching values between 0.01 and 0.02 for the sanded and polished samples. Due to the protective lubricant film, wear was minimal, and no

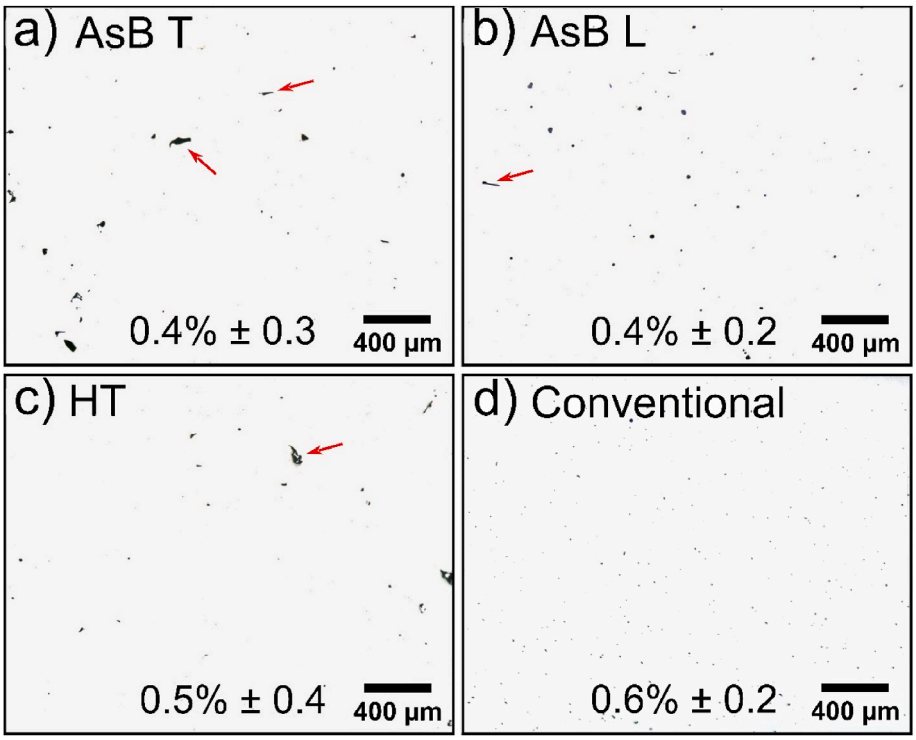

Fig. 3. OM images used for porosity analysis. Red arrows indicate defects such as lack of fusion and cracks. The numbers represent the calculated porosity for each sample. The gray background was artificially added to increase the visibility of the image.

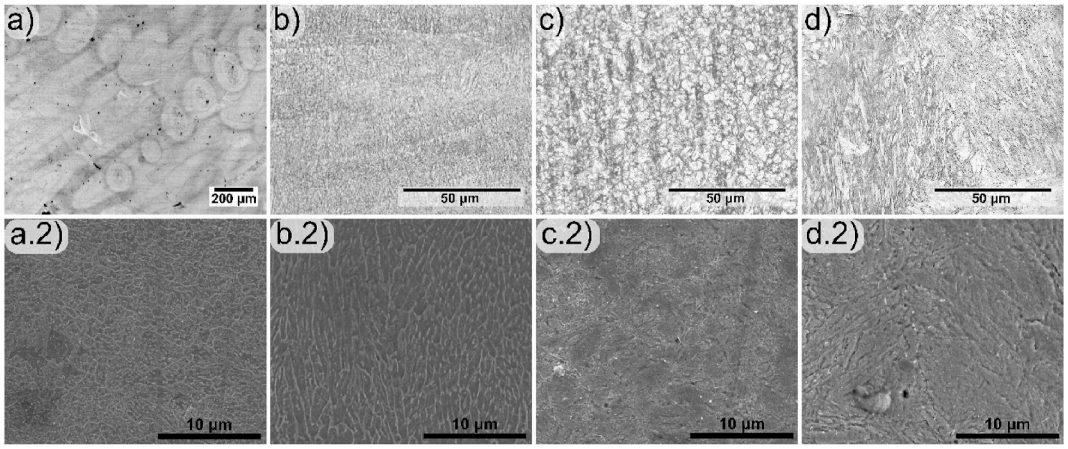

Fig. 4. OM and SEM images of the: a) AsB T; b) AsB L; c) HT and d) Conventional samples.

mass loss was detected, even within the 1 µg measurement range.

While the wear properties of conventionally processed H13 are well-explored in the literature, studies investigating H13 produced by AM remain comparatively scarce, despite the critical importance of wear resistance for this tool steel. Literature reviews have shown that, for conventionally processed H13, certain laser-based surface treatments can significantly enhance wear properties. Given the unique thermal cycles and rapid cooling rates inherent to L-PBF, this process holds promising potential to similarly influence wear behavior by generating a distinctive microstructure. Thus, understanding how L-PBF processing directly affects the wear properties of H13 is both relevant and timely for advancing applications of this material in high-wear environments.

The present work investigates the room-temperature wear resistance of H13 steel processed via laser powder bed fusion, analyzing both as-printed and post-heat treatment conditions as well as different build orientations. A comparative evaluation was performed against conventionally processed H13 (arc-melted), providing a baseline for performance. Additionally, detailed microstructural analyses were conducted to clarify the relationship between the manufacturing process and the resulting wear properties.

2. Experimental procedure

2.1. Laser powder bed fusion (L-PBF) process

The H13 powder, provided by LPW Technology Ltd (United Kingdom), was used to produce the samples in this study and had the following nominal chemical composition (wt %): Fe - 0.36C - 5.21Cr - 1.47Mo - 1.00Si - 0.40Mn – 0.90V. The powder exhibits a suitable granulometric distribution for the L-PBF process [7,9,12,20], with 70% of the particles below 35 µm and d_{50} between 25 and 30 µm. The morphology is approximately spherical, with the presence of some

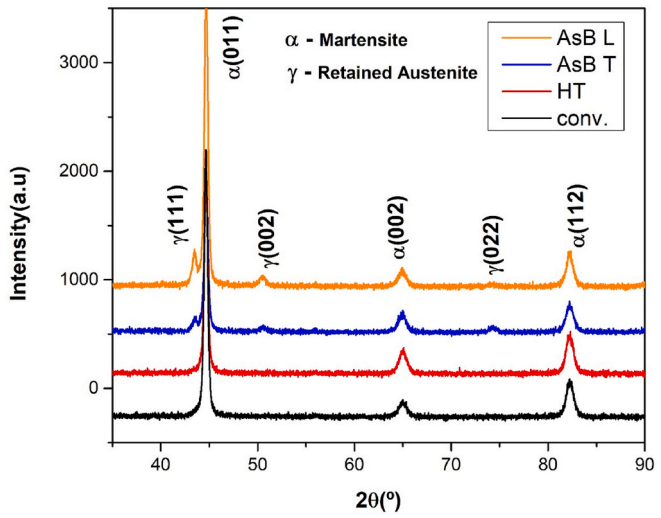

Fig. 5. X-ray diffraction patterns of analyzed samples.

Table 2
Wear rate, hardness and surface roughness for each condition tested. The maximum and minimum values represent the standard deviation.

Condition	AsB T	AsB L	HT	Conventional
Wear rate(mm^3/ N.m)	(1.7 ± 1.0) 10^{-4}	(1.2 ± 0.4) 10^{-4}	(3.0 ± 0.2) 10^{-4}	(2.2 ± 0.6) 10^{-4}
Hardness (HV)	556 ± 22	579 ± 18	547 ± 6	560 ± 21
Line roughness RA (μm)	0.010 ± 0.005	0.013 ± 0.009	0.012 ± 0.005	0.015 ± 0.011

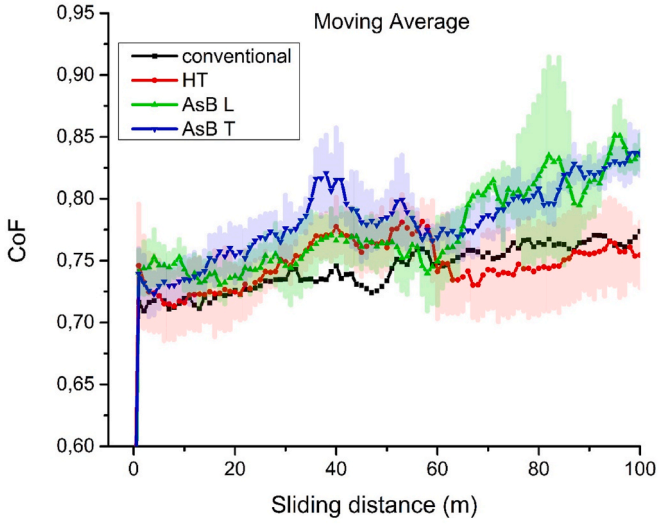

Fig. 6. Evolution of the Coefficient of friction (CoF) as a function of the sliding distance. The standard deviation of the conventional sample was omitted for better visualization of the graph. A complete image can be seen in the supplementary material.

satellite particles. A more detailed characterization of this powder has been previously conducted and presented in Ref. [11]. From this powder, six samples (10 × 20 × 20 mm) were printed using an AM OmniSint-160 additive manufacturing machine (OmniTek, Brazil) equipped with a Yb:YAG fiber laser with a maximum power of 400W. The parameters during the L-PBF process were as follows: power of 212 W, scanning speed of 580 mm/s, and 95 μm of hatching spacing. The scanning strategy employed in this work is illustrated in Fig. 1. It consists of 5 mm strokes with a rotation pattern of 32° between the layers. This strategy was selected based on its prior successful implementation in the same machine utilized for this study [21]. The parameters settings employed were derived from an optimization study published elsewhere [22].

2.2. Microstructural characterization

Three of the six printed samples were kept in the as-printed condition, while the other three underwent heat treatment. The heat treatment consisted of austenitizing at 1010 °C in a home-built furnace (accuracy of ±6 °C), followed by quenching in air and double tempering at 552 °C in a home-built electric furnace (accuracy of ± 5 °C). After that, all samples were prepared for microstructural characterization. The top surface, transverse to the build direction (Fig. 1), was sanded down and reduced by approximately three hundred microns, just enough to remove the effects of the last layers. Subsequently, the surface was polished with diamond paste (3 μm). The same was done with the side surface of the sample, parallel to the build direction. After polishing, five images were taken from different locations of each polished section for porosity quantification by optical microscopy using the software ImageJ. Additionally, the microstructure of these samples was examined using optical microscopy (Olympus BX41M-LED) after etching with Nital 2% and using a scanning electron microscope (SEM) Fei Quanta 400 microscope equipped with energy dispersive X-ray spectroscopy (EDX) detector.

The Vickers hardness of each sample was measured using an HMV Shimadzu microhardness tester. Five measurements were taken at various locations across the polished surface. Phase identification was conducted through X-ray diffraction using a Bruker model D8 Advance ECO X-ray diffractometer equipped with an SSD 160 high-speed detector. The phase fraction was calculated using Rietveld refinement with Maud software.

2.3. Tribological experimental procedures

The samples produced by AM were kept nearly at their original print size (10 × 20 × 20 mm) and tested under three different conditions on surfaces prepared beforehand during microstructural characterization. Firstly, the wear test was carried out on a surface perpendicular to the building direction (called As-Built Transversal – AsB T – see Fig. 2). In the second condition, the test was performed on a surface parallel to the building direction (Called As-Built Longitudinal – AsB L). Finally, the third condition was performed on a printed and thermally treated sample (called Heat-treated – HT). This sample was analyzed only on the surface perpendicular to the build direction because the heat treatment promotes a more isotropic structure and properties [23]. The heat treatment is the same as mentioned before. For comparison, a fourth sample was produced by electric arc melting in an argon atmosphere using an Edmund Bühler GmbH furnace. The sample removed from the arc furnace had an oblate spheroid shape. This sample was heat-treated and subsequently embedded in resin and cut approximately in half with a diamond disc. It was also ground, polished, and then characterized in the same manner as the other samples mentioned previously. This sample was called “conventional” (see Fig. 2).

Tribological tests were performed at room temperature on a Plint & Partners TE 67/R machine. The tests were of the reciprocal type in a ball-on-plate configuration, done in triplicate. The pin is made up of Al_2O_3. Table 1 shows the test conditions, which were almost all performed according to the standard (ASTM G133-05, “Procedure A”), except for the pin tip radius, which was 5.2 mm, instead of 4.76 mm. Note that the wear tests employed were not intended to accurately simulate any specific industrial application but rather to understand how different build directions and post-print heat treatment conditions can impact wear properties.

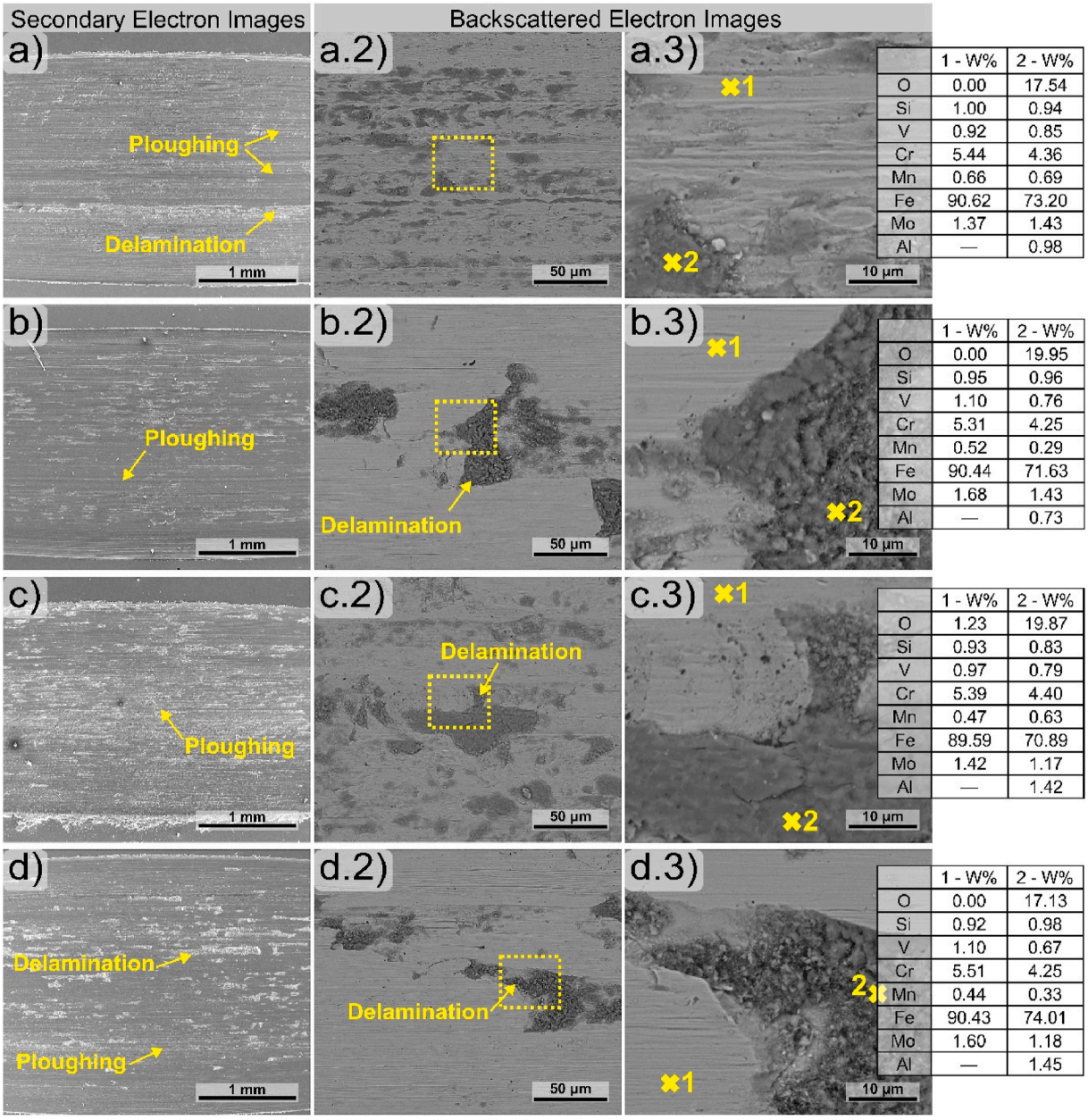

Fig. 7. SEM images of the worn surfaces after wear testing of a) AsB T b) AsB L; c) HT and d) Conventional samples.

The coefficient of friction (COF) was computed automatically. The volume loss was measured through 3D surface topography of the worn tracks using an Olympus LEXT OLS 4000 microscope. Surface roughness was also examined using confocal microscopy in three distinct regions for each sample. Each selected region had its roughness measured along seven horizontal and seven vertical lines, and an average was calculated afterward. The analyses of both the worn tracks and worn pins were performed using the same SEM device used for microstructural characterization. The alumina pins were coated with a thin layer of conductive paint to ensure effective grounding of electrons during sample analysis. The specific wear rate was calculated from formula K=V/(F·D), where V (mm^3) is the volume of material removed, F(N) is the normal load, and D (m) is the sliding distance.

3. Results

Fig. 3 shows some OM images used to quantify the porosity. It is possible to notice that, although the conventional sample presented a slightly higher porosity value (0.6%), this sample presents small and circular pores, uniformly distributed throughout the sample. The printed samples exhibit fewer defects (0.4%); however, their defects are larger (some greater than 100 µm), with irregular shapes and sharp edges.

Fig. 4 shows the microstructure of samples under different processing conditions and heat treatments. In the Asb T samples (Fig. 4 – a)) one can see the melting pools marks seen from above. The image a.2 shows a cellular microstructure of H13 steel when processed by L-PBF. Fig. 4 – b) shows sample Asb L at higher magnification to improve detail visualization. The marks from the molten pools are still visible in a longitudinal section. Image b.2 displays the characteristic cell morphology of this condition. The microstructure of the Asb T and Asb L conditions is quite similar. Fig. 4 - c) shows the HT sample. The heat treatment applied to this sample eliminated the cellular morphology characteristic of the L-PBF process, promoting grain growth and resulting in a coarser microstructure compared to the AsB samples. Fig. 4 – d) shows the conventional sample, which exhibits the coarsest microstructure among all samples, with distinguishable martensite laths. This is attributed to the

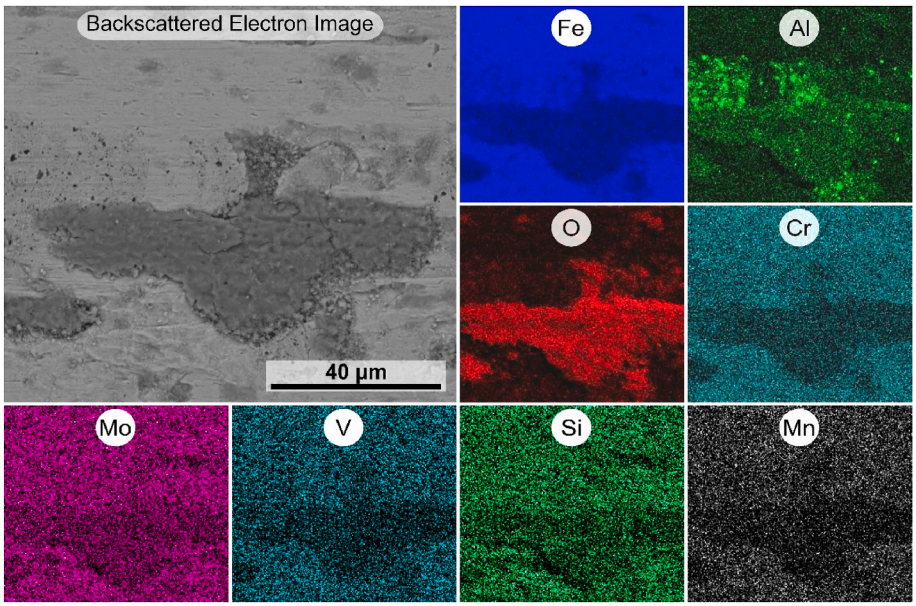

Fig. 8. Elements map made by EDX on the worn surface of the HT sample.

cooling rate of arc melting, which is lower than that of the L-PBF process. Even after heat treatments, the conventional sample retains a coarser microstructure compared to the HT sample. However, despite the differences in refinement, images c.2) and d.2) show that the HT and Conventional samples have the same phases, which consist of tempered martensite with some dispersed carbides in the matrix.

Fig. 5 shows the X-ray diffraction results for samples under different conditions. The patterns confirm the presence of retained austenite along with martensite in the as-built samples and only martensite in the heat-treated and conventional samples.

Table 2 presents the wear rate, hardness, and surface roughness values (measured using confocal microscopy) observed under each of the tested conditions. The AsB L sample exhibited the lowest specific wear rate (1.2×10^{-4} mm³/N·m), while the HT sample showed the highest value (3.0×10^{-4} mm³/N·m).

Fig. 6 shows the evolution of the COF of the samples as a function of the sliding distance during the wear test. Each curve was obtained from the average of the three tests performed for each sample. The shadow behind each curve represents the standard deviation. The COF of all samples started around 0.74 and increased slightly as the test progressed. After half the distance the COF of the as-printed samples tends to increase a little more, ending the test around 0.82.

Fig. 7 displays SEM images of the worn tracks along with semi-quantitative EDX analysis. In the higher magnification images, it is possible to observe signs of abrasion, plastic deformation, and delamination. Image c), corresponding to the HT sample, shows a greater number of delamination craters. The EDX analyses of the samples reveal low values of oxygen (O) on the smooth contact surface and a high concentration of oxygen in the debris accumulated within delamination craters.

Fig. 8 shows an SEM-EDX mapping of the worn track of the HT sample. A high concentration of oxygen, iron and aluminum can be observed in the darker region.

Fig. 9 shows the SEM images of the alumina pins after the wear tests. Note the presence of two phases, one darker and another lighter. EDX analyses show that the clearest region is H13 adhered to the surface of the pin. The darkest region is the pin (Al2O3). Fig. 10 displays an element map of the AsB T sample, confirming the elements of the adhered material. In the image, it is possible to notice that there was plastic deformation of the H13 adhered to the surface of the pin.

4. Discussion

It is known that H13, when processed through the L-PBF process, presents 10–25% of retained austenite, depending on the combination of process parameters [11,24,25]. Austenite forms during the solidification stage, where the cellular growth of delta ferrite (δ) rejects solute, causing the segregation of alloying elements like C, Cr, and Mo along the cell walls. As cooling progresses, the delta ferrite (δ) transforms into solute-depleted austenite, which later becomes martensite. However, the austenite formed along the cell walls, enriched in solute and with a lower Ms point, remains retained at room temperature [21,23,24]. A small amount of austenite may also remain retained within the cells, between the martensite laths, after cooling [11,26,27].

In the present work, the retained austenite fraction calculated through Rietveld refinement was 13.0% ± 0.4 (The quality indicators of the curve fitting are shown in the supplementary material). Since the retained austenite is a softer phase, it is expected that its presence causes a reduction in the hardness of the printed H13 when compared with a conventional processed H13. However, the H13 processed by L-PBF presented hardness like the conventional one. These results are in agreement with studies in the literature [7,23].

The hardness of L-PBF processed H13, comparable to conventional fully martensitic H13, is explained by its finer microstructure, produced by the high cooling rates imposed by laser melting, and by the presence of lightly tempered martensite. As demonstrated by Li et al. [26], for as-printed H13 steel, the primary contribution to mechanical strength comes from the high dislocation density, followed by grain boundary strengthening. After H13 undergoes quenching and tempering heat treatments, the contribution of dislocation density decreases slightly compared to the as-printed condition, but it still represents the largest share. However, in this case, the second largest contribution comes from precipitation hardening, rather than grain boundary strengthening, due to grain growth during heat treatments. This may explain why the HT sample showed a slight decrease in hardness compared to the printed sample, but it still exhibits hardness comparable to the Conventional sample, considering the standard deviation. It is worth noting that the heat treatment, in addition to causing a shift in the order of the main strengthening mechanisms of the material, also promotes the dissolution of retained austenite by better homogenizing the distribution of elements during austenitization, quenching and tempering [24,26]. However, explaining these mechanisms in detail is beyond the scope of this

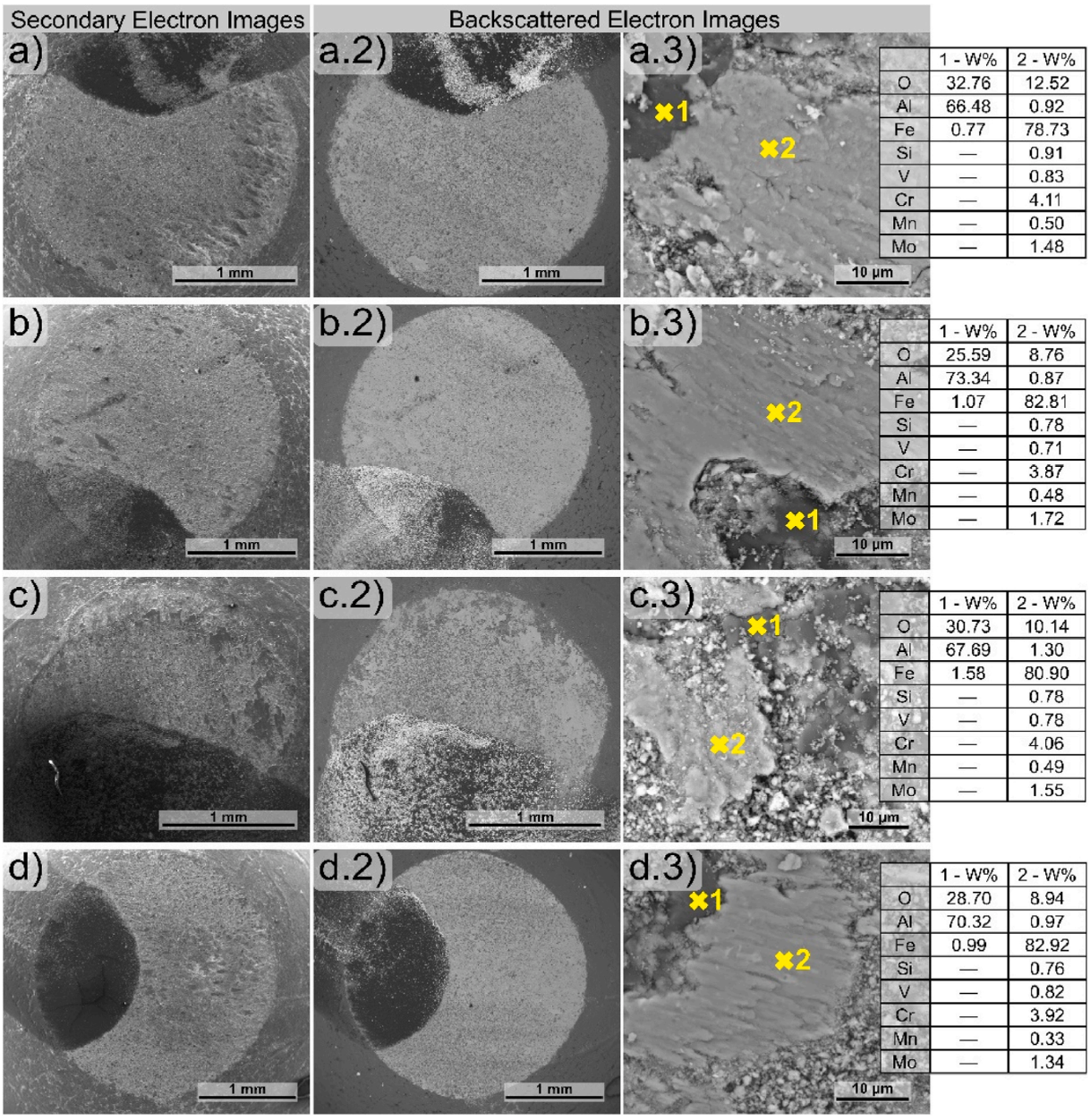

Fig. 9. SEM images of the Alumina pin tip after wear testing: a) AsB T; b) AsB L; c) HT; d) Conventional. The dark spots on the edges of the pins are from the conductive ink used to enhance the electron conductivity during the SEM analysis.

work. Further information can be found in the cited references.

During the wear tests, all samples initially displayed a comparable coefficient of friction (COF), ranging between 0.7 and 0.75, with a gradual increase observed as the test progressed. However, a distinction between the samples became noticeable after covering half of the testing distance. The thermally treated samples completed the test with a COF of approximately 0.75, whereas the as-printed samples exhibited a higher COF, exceeding 0.8. The relatively elevated COF values suggest the presence of an adhesion mechanism [14,15], so the as-printed samples may be experiencing slightly more adhesion compared to the thermally treated samples. Further explanation will be provided.

Adhesion occurs when some asperities of one surface join with the asperities of another surface, forming microjoints. This phenomenon can be favored depending on temperature conditions, load, pressure, lubrication, or chemical affinity between the two surfaces [29]. When the two adhered surfaces enter relative motion, adhesive wear can occur, where material from one surface can be transferred to the other surface and vice versa. Since more force is required to break the microjoints during adhesive wear, the presence of this mechanism is one of the main contributors to a high coefficient of friction [28]. In the present study, EDX analyses revealed no oxide layer formation on the worn tracks, which could prevent adhesive wear (see Fig. 7). This outcome aligns with existing literature on conventionally processed H13 tested at room temperature [15,30]. Additionally, EDX analyses of the pins confirmed H13 transfer, corroborating the occurrence of adhesion (see Fig. 9).

In pin-on-disc tests, it has been previously observed that the COF of conventionally processed H13 can increase during testing due to intrinsic tempering from frictional heating, as noted by Bahrami et al. [14]. They found evidence of tempering in tests conducted at a load of 98 N, where the COF progressively increased due to heat accumulation and temperature rise—an effect not observed at lower loads. Their setup used a steel pin (65 HRC), which resulted in lower COF values. In a reciprocating test with a relatively short sliding distance, as in the present study, localized temperature buildup is expected, likely causing

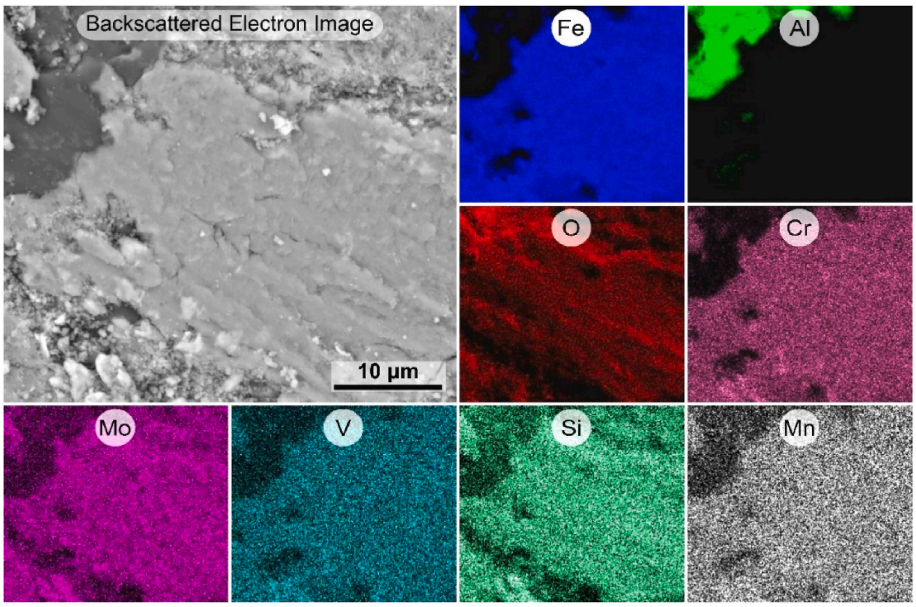

Fig. 10. SEM-EDX mapping of alumina pin after dry-reciprocating sliding on the AsB T sample.

similar heating and tempering effects. This heating particularly impacts retained austenite, which, being more ductile and more susceptible to softening at elevated temperatures than martensite, may increase the susceptibility to adhesive wear. This mechanism contributes to the gradual rise in COF in the as-printed samples, as the softer retained austenite promotes material transfer and adhesion at the contact interface. In contrast, the heat-treated samples, with a reduced fraction of retained austenite, exhibit a more stable COF throughout the test.

Despite the final COF being slightly elevated, the as-printed samples exhibited a slightly lower wear rate compared to the others. Sample AsB L showed the lowest wear rate (1.2×10^{-4} mm³/N.m). However, the values are very close to the wear rate values of the conventional sample, considering the standard deviation (See Table 2). When the sample processed by L-PBF undergoes the same heat treatment (HT sample), its wear rate becomes slightly higher ($3{,}0 \times 10^{-4}$ mm³/N.m) than the wear rate of conventionally processed H13. This behavior may be the result of microstructural defects caused by the L-PBF process, as shown in Fig. 3. A more detailed explanation involves understanding the wear mechanisms.

In addition to the adhesion mechanism explained earlier (see Fig. 9), all samples also exhibited signs of abrasion and delamination (See Fig. 7). Delamination can often be associated with the formation of an oxide layer [15,31], but not always. As proposed by Suh [32], during wear the layer just below the surface undergoes more cold work than the interface. As wear progresses, dislocations accumulate at a finite distance from the surface, forming voids. Over time, the voids become cracks parallel to the sliding surface, and when they reach a critical length, delamination occurs. If there are second-phase particles, this mechanism is accentuated. The same is true for defects. Since samples of H13 processed by L-PBF may show solidification cracks [11], adhesion failures between layers [33], and irregular defects with acute angles (Fig. 3), these defects are preferred points for stacking dislocations, accentuating the mechanism of delamination. This explains why the printed and heat-treated sample (HT) performed worse than the "conventional" sample during wear tests, despite these two samples undergoing the same heat treatment and having similar microstructures.

Since the Asb L and Asb T samples exhibit similar defects to the HT sample, one might expect them to show a higher level of delamination as well. However, their greater microstructural refinement, unaffected by thermal treatment, enhances toughness and thereby increases resistance to delamination. Additionally, the HT sample contains precipitated carbides from the tempering process, which may act as dislocation nucleation sites, further intensifying delamination. These combined factors could explain why the printed samples performed slightly better in wear tests, despite all samples exhibiting similar wear mechanisms and comparable performance within the standard deviation. This comparable performance across treatments demonstrates the feasibility of producing complex geometries through additive manufacturing while retaining the wear properties of H13 steel, regardless of the heat treatment. Consequently, these findings open the possibility of using parts in the as-printed condition depending on the application, which could reduce costs associated with heat treatment and establish a new processing route for producing complex parts.

5. Conclusion

H13 tool steel was processed by L-PBF and subjected to reciprocal, unlubricated wear test against Al2O3 pin in a sphere-on-plate configuration, before and after heat treatments, and then compared with the same material processed conventionally. The following conclusions can be taken:

- All conditions tested showed the same wear mechanisms, which were delamination, abrasion, and adhesion. No oxide layer formation was observed.
- The coefficient of friction of the samples increased slightly during the test. For the heat-treated samples, it ranged from 0.7 to 0.75, whereas for the as-printed samples, it ranged from 0.7 to 0.85. This difference can be attributed to the retained austenite present in these samples, which is more susceptible to in-situ tempering effects on the contact surface.
- The wear rate does not vary significantly between the parallel and perpendicular planes to the building direction of the part.
- The as-printed samples showed a slightly lower wear rate (1.7×10^{-4} and 1.2×10^{-4} mm³/N.m) than the conventional sample (2.2×10^{-4} mm³/N.m), due to its greater microstructural refinement.
- The printed and heat-treated sample had a slightly higher wear rate (3.0×10^{-4} mm³/N.m) than the conventional sample, due to intrinsic defects in the printing process.

Declaration of competing interest

The authors declare that they have no known competing financial interests or personal relationships that could have appeared to influence the work reported in this paper.

Acknowledgments

This study was financed in part by the Coordenação de Aperfeiçoamento de Pessoal de Nível Superior - Brazil (CAPES) - Finance Code 001. The authors would like to thank the São Paulo Research Foundation (FAPESP) for the financial support received through project numbers 2016/11309-0, 2017/27031-4, and 2018/15659-1. Tales is grateful for the support of the Brazilian National Council for Scientific and Technological Development (CNPq) under grant no. 163263/2020–5. The authors are also grateful to Omnitek for the support with the preparation of the LPBF samples and the Laboratory of Structural Characterization (LCE-DEMa-UFSCar) for the general facilities.

Appendix A. Supplementary data

Supplementary data to this article can be found online at https://doi.org/10.1016/j.jmrt.2024.12.012.

References

[1] Mesquita RA. Tool steels: properties and performance. first ed. New York: CRC Press; 2016. https://doi.org/10.1201/9781315181516.
[2] International A. ASM handbook volume 1: properties and selection: irons, steels, and high-performance alloys, vol. 1; 1990. p. 3470.
[3] DebRoy T, Mukherjee T, Milewski JO, Elmer JW, Ribic B, Blecher JJ, et al. Scientific, technological and economic issues in metal printing and their solutions. Nat Mater 2019;18:1026–32. https://doi.org/10.1038/s41563-019-0408-2.
[4] DebRoy T, Wei HL, Zuback JS, Mukherjee T, Elmer JW, Milewski JO, et al. Additive manufacturing of metallic components – process, structure and properties. Prog Mater Sci 2018;92:112–224. https://doi.org/10.1016/j.pmatsci.2017.10.001.
[5] Bajaj P, Hariharan A, Kini A, Kürnsteiner P, Raabe D, Jägle EA. Steels in additive manufacturing: a review of their microstructure and properties. Mater Sci Eng, A 2019;772:138633. https://doi.org/10.1016/J.MSEA.2019.138633.
[6] Mazur M, Brincat P, Leary M, Brandt M. Numerical and experimental evaluation of a conformally cooled H13 steel injection mould manufactured with selective laser melting. Int J Adv Manuf Technol 2017;93:881–900. https://doi.org/10.1007/s00170-017-0426-7.
[7] Ren B, Lu D, Zhou R, Li Z, Guan J. Preparation and mechanical properties of selective laser melted H13 steel. J Mater Res 2019;34:1415–25. https://doi.org/10.1557/jmr.2019.10.
[8] Lee J, Choe J, Park J, Yu JH, Kim S, Jung ID, et al. Microstructural effects on the tensile and fracture behavior of selective laser melted H13 tool steel under varying conditions. Mater Char 2019;155:109817. https://doi.org/10.1016/j.matchar.2019.109817.
[9] Yan J, Song H, Dong Y, Quach WM, Yan M. High strength (~2000 MPa) or highly ductile (~11%) additively manufactured H13 by tempering at different conditions. Mater Sci Eng, A 2020;773:138845. https://doi.org/10.1016/j.msea.2019.138845.
[10] Chen CJ, Yan K, Qin L, Zhang M, Wang X, Zou T, et al. Effect of heat treatment on microstructure and mechanical properties of laser additively manufactured AISI H13 tool steel. J Mater Eng Perform 2017;26:5577–89. https://doi.org/10.1007/s11665-017-2992-0.
[11] Oliveira AP, Lima LHQR, Felipe BC, Bolfarini C, Coelho RT, Gargarella P. Effect of microstructure and defect formation on the bending properties of additive manufactured H13 tool steel. J Mater Res Technol 2021. https://doi.org/10.1016/j.jmrt.2021.10.011.
[12] Narvan M, Al-Rubaie KS, Elbestawi M. Process-structure-property relationships of AISI H13 tool steel processed with selective laser melting. Materials 2019;12:1–20. https://doi.org/10.3390/ma12142284.
[13] Yan JJ, Chen MT, Quach WM, Yan M, Young B. Mechanical properties and cross-sectional behavior of additively manufactured high strength steel tubular sections. Thin-Walled Struct 2019;144:106158. https://doi.org/10.1016/j.tws.2019.04.050.
[14] Bahrami A, Anijdan SHM, Golozar MA, Shamanian M, Varahram N. Effects of conventional heat treatment on wear resistance of AISI H13 tool steel. Wear 2005;258:846–51. https://doi.org/10.1016/j.wear.2004.09.008.
[15] Wei MX, Wang SQ, Wang L, Cui XH, Chen KM. Effect of tempering conditions on wear resistance in various wear mechanisms of H13 steel. Tribol Int 2011;44:898–905. https://doi.org/10.1016/j.triboint.2011.03.005.
[16] Chen L, Zhou H, Zhao Y, Ren LQ, Li XZ. Abrasive particle wear behaviors of several die steels with non-smooth surfaces. J Mater Process Technol 2007;190:211–6. https://doi.org/10.1016/j.jmatprotec.2007.02.043.
[17] Telasang G, Dutta Majumdar J, Padmanabham G, Manna I. Wear and corrosion behavior of laser surface engineered AISI H13 hot working tool steel. Surf Coating Technol 2015;261:69–78. https://doi.org/10.1016/j.surfcoat.2014.11.058.
[18] Patra Karmakar D, Gopinath M, Nath AK. Effect of tempering on laser remelted AISI H13 tool steel. Surf Coating Technol 2019;361:136–49. https://doi.org/10.1016/j.surfcoat.2019.01.022.
[19] Guenther E, Kahlert M, Vollmer M, Niendorf T, Greiner C. Tribological performance of additively manufactured aisi h13 steel in different surface conditions. Materials 2021;14:1–10. https://doi.org/10.3390/ma14040928.
[20] Yan J, Zhou Y, Gu R, Zhang X, Quach WM, Yan M. A comprehensive study of steel powders (316L, H13, P20 and 18Ni300) for their selective laser melting additive manufacturing. Metals 2019;9. https://doi.org/10.3390/met9010086.
[21] Fonseca EB, Gabriel AHG, Araújo LC, Santos PLL, Campo KN, Lopes ESN. Assessment of laser power and scan speed in fl uence on microstructural features and consolidation of AISI H13 tool steel processed by additive manufacturing. Addit Manuf 2020;34:101250. https://doi.org/10.1016/j.addma.2020.101250.
[22] Oliveira AP, Figueira G, Coelho RT, Bolfarini C, Gargarella P. Application of the box-behnken design in the optimization of laser powder bed fusion of H13 tool steel. Mater Res 2023;26. https://doi.org/10.1590/1980-5373-mr-2023-0250.
[23] Krell J, Röttger A, Geenen K, Theisen W. General investigations on processing tool steel X40CrMoV5-1 with selective laser melting. J Mater Process Technol 2018;255:679–88. https://doi.org/10.1016/j.jmatprotec.2018.01.012.
[24] Fonseca EB, Escobar JD, Gabriel AHG, Ribamar GG, Boll T, Lopes ÉSN. Tempering of an additively manufactured microsegregated hot-work tool steel: a high-temperature synchrotron X-ray diffraction study. Addit Manuf 2022;55. https://doi.org/10.1016/j.addma.2022.102812.
[25] Deirmina F, Peghini N, AlMangour B, Grzesiak D, Pellizzari M. Heat treatment and properties of a hot work tool steel fabricated by additive manufacturing. Mater Sci Eng, A 2019;753:109–21. https://doi.org/10.1016/j.msea.2019.03.027.
[26] Li S, Yang S, Zhao Y, Dong Y, Wang Z. 2 GPa H13 steels fabricated by laser powder bed fusion and tempering: microstructure, tensile property and strengthening mechanism. Mater Sci Eng, A 2023;888:145803. https://doi.org/10.1016/j.msea.2023.145803.
[27] Tan Q, Yin Y, Wang F, Chang H, Liu S, Liang G, et al. Rationalization of brittleness and anisotropic mechanical properties of H13 steel fabricated by selective laser melting. Scripta Mater 2022;214:114645. https://doi.org/10.1016/j.scriptamat.2022.114645.
[28] Blau PJ. ASM handbook, volume 18 - friction, lubrication, and wear Technology. ASM International.;n.d.
[29] Podgornik B. Adhesive wear failures. J Fail Anal Prev 2022;22:113–38. https://doi.org/10.1007/s11668-021-01322-4.
[30] Uma Devi M, Chakraborty TK, Mohanty ON. Wear behaviour of plasma nitrided tool steels. Surf Coating Technol 1999;116–119:212–21. https://doi.org/10.1016/S0257-8972(99)00118-8.
[31] Wang SQ, Wei MX, Wang F, Cui XH, Chen KM. Effect of morphology of oxide scale on oxidation wear in hot working die steels. Mater Sci Eng, A 2009;505:20–6. https://doi.org/10.1016/j.msea.2008.10.032.
[32] Suh NP. Update on the delamination theory of wear, vol. 25; 1981. p. 111–24.
[33] Sun Y, Wang J, Li M, Wang Y, Li C, Dai T, et al. Thermal and mechanical properties of selective laser melted and heat treated H13 hot work tool steel. Mater Des 2022;224:111295. https://doi.org/10.1016/j.matdes.2022.111295.